




On the high-energy electron beam irradiation-induced defects in Cu_2SnSe_3 system: an effort towards modifying the structure, microstructure, and thermoelectric transport

K. Gurukrishna¹, Suraj Mangavati¹, Ashok Rao^{1,*} , P. Poornesh¹, Vikash Chandra Petwal², Vijay Pal Verma², and Jishnu Dwivedi²

¹Centre for Clean Energy, Department of Physics, Manipal Institute of Technology, Manipal Academy of Higher Education, Manipal 576104, India

²Industrial Accelerator Section, PSIAD, Raja Ramanna Centre for Advanced Technology, Indore, M.P. 452012, India

Received: 1 July 2022

Accepted: 26 August 2022

Published online:

7 September 2022

© The Author(s) 2022

ABSTRACT

We present report on modulating thermoelectric transport in Cu_2SnSe_3 system via irradiating high-energy electrons of energy of about 8 MeV. Electrical transport is investigated at near room to mid-temperature regime (300–700 K). A smooth transition from degenerate to non-degenerate type of conductivity is observed in all the samples, which indicates the injection of minority carriers with ionisation of defects at high temperatures. Defects created through the knock-on displacement of the constituent atoms is successful in promoting the power factor in the material. Cu_2SnSe_3 irradiated with 50 kGy is found to achieve highest power factor of $228 \mu\text{W}/\text{mK}^2$ at 700 K, which is nearly 20% higher than the power factor of pristine material at the same temperature.

1 Introduction

Thermoelectric (TE) materials have emerged as promising candidates for renewable energy technology that is capable in harvesting electricity by the temperature gradient. Reciprocally dependent electronic and thermal transport parameters can be related to the figure of merit (ZT) that defines the thermoelectric performance of a material which is given by [1]

$$ZT = \frac{S^2 \sigma T}{\kappa}, \quad (1)$$

where S is Seebeck coefficient, σ and κ are electrical and thermal conductivities, respectively. Balancing these entangled properties is a major challenge to have a good TE material. The optimal electronic transport depends primarily on the weighted mobility μ_w , which in turn varies with the density of states effective mass m^* . Recently, Snyder et al. [2] have proposed an equation which can be used to deduce

Address correspondence to E-mail: ashokanu_rao@rediffmail.com

temperature-dependent weighted mobility via connecting the electrical conductivity (σ) and Seebeck coefficient (S) which is given by

$$\mu_w = \frac{3h^3\sigma}{8\pi e(2m_e k_B T)^{3/2}} \left(\frac{\exp\left[\frac{|S|}{k_B/e} - 2\right]}{1 + \exp\left[-5\left(\frac{|S|}{k_B/e} - 1\right)\right]} + \frac{\frac{3}{\pi^2} \frac{|S|}{k_B/e}}{1 + \exp\left[5\left(\frac{|S|}{k_B/e} - 1\right)\right]} \right) \quad (2)$$

here μ_w is directly related to the thermoelectric quality factor B i.e. $\mu_w \propto B$ which turns out to be an essential factor that decides the superior thermoelectric behaviour in any material. Hence, modulating μ_w is one of the ways to enhance the power factor [3].

Cu_2SnSe_3 is a diamond-structured narrow band gap semiconductor of I–IV–VI family of materials in which Cu–Se bond facilitates degenerate electronic transport. Three-dimensional bond network with five possible tetrahedra makes Cu_2SnSe_3 highly conductive in comparison with the state-of-the-art TE materials systems like SiGe, SiC, etc. [4, 5]. Sn atom residing inside the network of Cu–Se promotes the phonon scattering, thereby fulfilling the criteria of phonon glass electron crystal (PGEC). This facilitates the low thermal conductivity in Cu_2SnSe_3 as compared to the most of binary chalcogenide systems [6]. Cu_2SnSe_3 is found to crystallise into different allotropic forms viz. cubic, monoclinic, and rhombohedral [7–9], which depends on the method of synthesis. Since Sn atom in the crystal contributes to the electronic transport, most of the efforts done to optimise the charge transport are at Sn site [5]. It was found to be an effective dopant in enhancing the power factor and hence the highest ZT is reported for In-doped samples [5, 10, 11]. Elemental doping [12, 13], composites [14, 15], and tuning in stoichiometry [16, 17] are promising strategies in promoting the thermoelectric behaviour in these systems. Other than elemental replacement and introducing secondary phases, irradiating the materials is found to show a direct effect on the structure and other electrophysical properties [18–20]. Displacement of constituent atoms via knocking them on to the defect states has been reported using low-energy electrons [21]. Electron beam is used in various

carbon-based nanostructured materials to modulate the structural properties [18, 22]. Literature also reports that electron beam irradiation can modify transport properties in perovskite metal oxides [23, 24]. Takashiri et al. [25] have done studies using 0.17 MeV electron beam on Bi–Sb–Te nanocrystalline films. They observed an increase in power factor of the system. Electron irradiation (8 MeV)-induced defects in Bi_2Se_3 are reported by Saji et al. [26], which demonstrates an increase in the carrier density. It is evident from the literature that the electron beam irradiation is one of the effective ways in modifying the electronic transport in thermoelectric semiconductors. There are not many reports on the influence of electron-induced defects on thermoelectric materials especially in diamond-structured Cu-based materials. The present report deals with a novel *ex-situ* approach to modify the structure and microstructure so as to improve the TE performance via inducing the crystal distortion through knock-on displacement of atoms by high-energy electrons.

2 Experimental details

Polycrystalline samples of Cu_2SnSe_3 were synthesised via conventional solid-state reaction route. Highly pure (4 N) elemental powders of Cu (Loba chemie), Se (Sigma Aldrich), and Sn (Sigma Aldrich) were weighed according to the nominal stoichiometry and blended well in agate mortar for about 2 h. The blended powder was compacted into rectangular pellets of dimension 11 mm × 6 mm × 2 mm using a uniaxial hydraulic press with Tungsten carbide die. The pellets were encapsulated inside quartz ampoule at high vacuum (10^{-6} mbar) and then sintered at 773 K for 72 h followed by natural cooling. The metallurgical process was repeated with a sintering temperature of 523 K for 24 h to obtain good quality densified pellets with homogeneity. Samples from the same branch were exposed to electron beam of energy 8 MeV with a fluence of 10^{14} cm⁻² using a Linear accelerator (LINAC). The samples were irradiated with a dosage of 50 kGy, 100 kGy, and 150 kGy. The stopping power and CSDA range of the radiation are calculated using ESTAR program. For Cu_2SnSe_3 samples with density of 3.80 g/cm³, stopping power is found to be 1.886 MeV g/cm² and

CSDA range is 5.205 g/cm². To confirm the phase formation, X-ray diffraction was performed at room temperature (Rigaku miniflex 600 5G). Rietveld analysis of the XRD profile was carried to derive crystallographic information of the pure and electron-irradiated samples. Using EVO MA18 Scanning electron microscope, the topographical details of the samples were inspected. Elemental distribution in the samples was analysed using Oxford EDS system attached to the SEM. Simultaneous high-temperature electrical resistivity and Seebeck coefficient measurements were done using Linseis LSR-3 system. Hall effect measurements were performed at room temperature using Ecopia HMS-5500 Hall measurement system employing van der Pauw geometry using InSn alloy ohmic contacts.

3 Results and discussions

3.1 Phase formation and microstructure

The XRD peaks of Cu₂SnSe₃ sample were indexed to JCPDS card #04-002-6015 [7], which shows the crystallisation of the material into cubic sphalerite-type structure consisting of the space group $F\bar{4}3m$. No changes in the structure were observed due to electron irradiation. The quantitative analysis of the phase was done using Rietveld analysis using Fullprof suite. The line profile was generated for cubic Cu₂SnSe₃ system with Pseudo-Voigt peak profile. The background variation is defined by a set of points with refinable heights. The obtained goodness-of-fit values verify the well fitting of experimental data with the generated line profile (see Fig. 1).

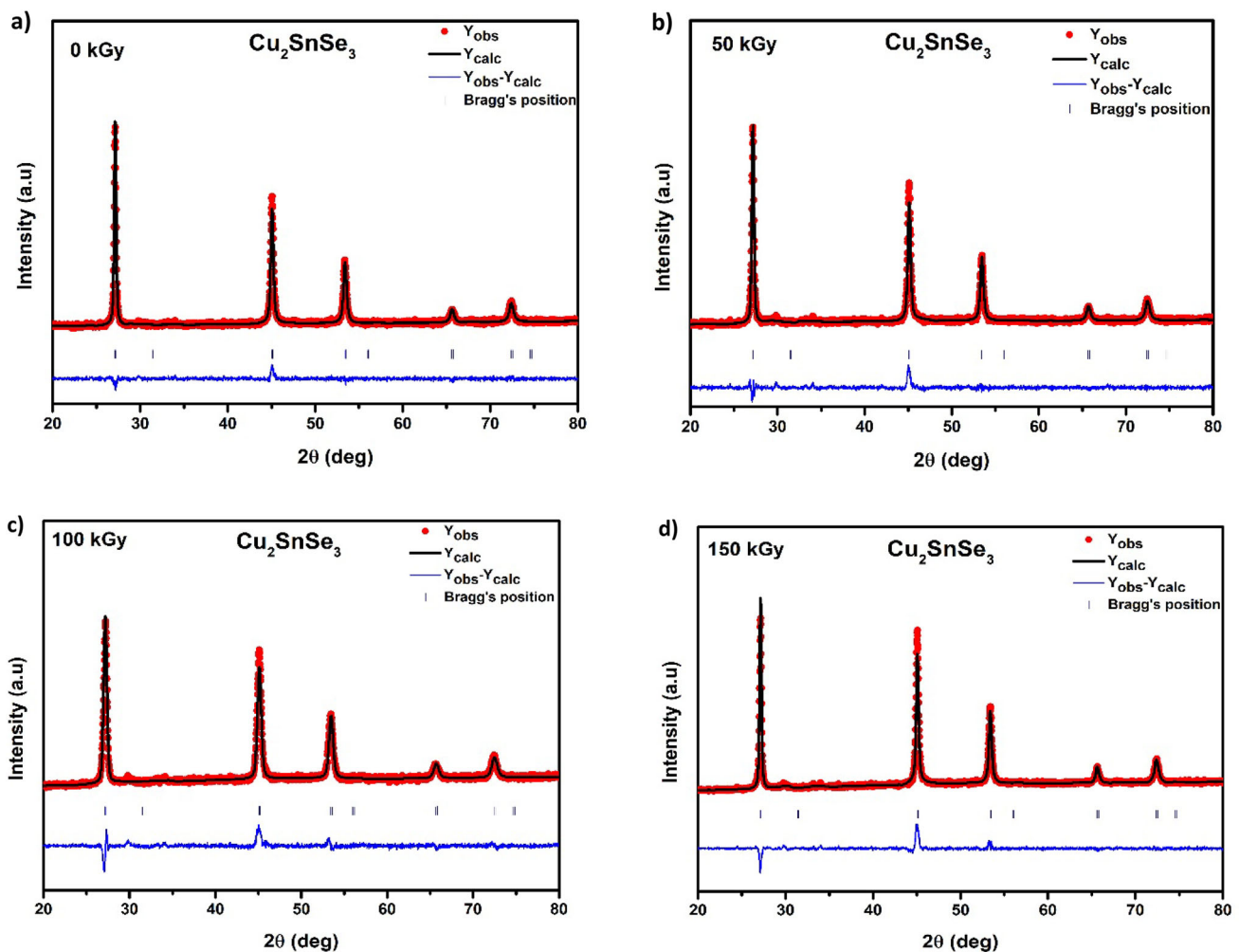


Fig. 1 Rietveld refined graphs of Cu₂SnSe₃ samples irradiated with **a** 0 kGy, **b** 50 kGy, **c** 100 kGy, **d** 150 kGy

Table 1 Crystallographic information by Rietveld analysis of Cu₂SnSe₃ irradiated with different electron beam dosages

Irradiation dosage	0 kGy	50 kGy	100 kGy	150 kGy
System	Cubic	Cubic	Cubic	Cubic
Space group	F $\bar{4}3m$	F $\bar{4}3m$	F $\bar{4}3m$	F $\bar{4}3m$
$a = b = c$	5.688(6)	5.683(5)	5.683(7)	5.688(1)
$\alpha = \beta = \gamma$	90	90	90	90
GoF index	1.2	1.3	1.4	1.5
χ^2	1.3	1.6	1.9	2.3
Maximum energy transferred E_M (keV)	Cu	Sn	Se	
	2.3	1.3	1.9	

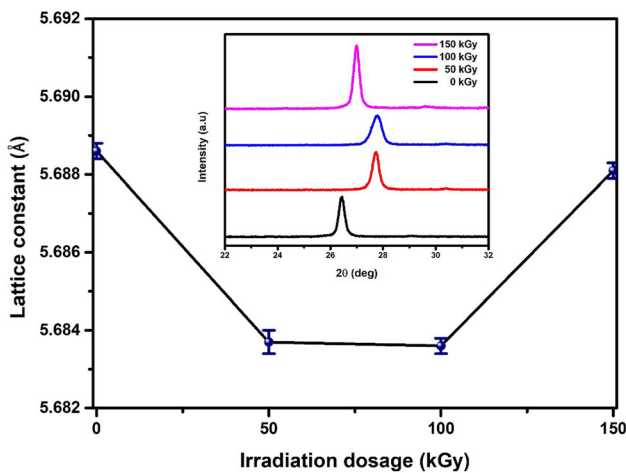


Fig. 2 Variation of lattice constants with irradiation dosage. Inset shows the major peak shift of pristine and irradiated Cu₂SnSe₃ samples

Crystallographic information with fit parameters is provided in Table 1. Shifting of the XRD peaks towards higher angle is noticed as the irradiation dosage is increased to 50 and 100 kGy beyond which the retrieving up of the peaks could be observed for the sample irradiation dosage 150 kGy as shown in Fig. 2. This behaviour is clearly reflected in the lattice constants, showing the distortion in the lattice with increasing irradiation dosage. The maximum energy transferred, E_M , into the constituent atom of mass m_a from an electron of mass m_e with kinetic energy E is given by [25]

$$E_M = \frac{2m_a E(E + 2m_e c^2)}{[(m_a + m_e)^2 c^2 + 2m_a E]}, \tag{3}$$

where c is the speed of light. The evaluated E_M values are listed in Table. 2. Since the displacement energy

values are found to be high, we presume the formation of knock-on displacement of the atoms thereby creating the point defects [21, 27].

SEM micrographs (Fig. 3) depict the densified microstructure of the synthesised samples with less visible porosities. Irregular growth of the agglomerated grain is identified in all the samples. Elemental distribution in the samples is found to be homogeneous with the recommended stoichiometry as per the EDS analysis as shown in Fig. 4. Even though well-defined changes could not be observed in the microstructure, the nano-level dots noted in the samples bombarded with higher dosage demonstrates the piercing of the high-energy electrons.

3.2 Electrical transport

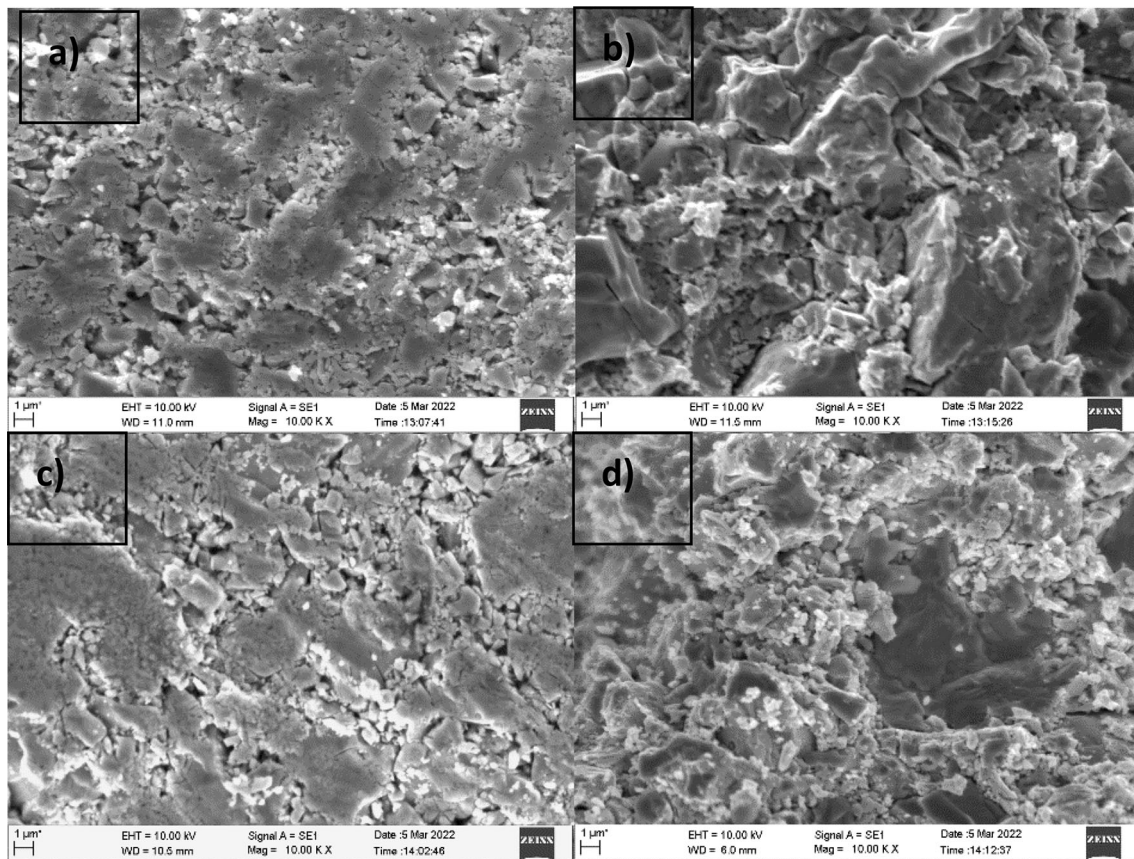
The electrical resistivity of all the samples is measured in the temperature regime 300–700 K, which is shown in Fig. 5a. Electrical resistivity data show that it initially increases with the increase in temperature up to an optimal temperature (~ 450 K), above which it is observed to reduce with further rise in temperature. The slump in the resistivity seen in all the samples at high temperatures signify a smooth transition from degenerate to non-degenerate semi-conducting behaviour. Possibility of the diffusion of minority carriers along with ionisation of the defects triggered at high temperatures could be the reason for the observed temperature dependency of charge transport [28, 29]. We suspect the hopping of small polarons at high temperatures where there can be a possibility of rise in phonon hopping rate in an Arrhenius manner. Hence, to explain the intrinsic nature of semiconducting behaviour of $\rho(T)$ Arrhenius equation is used with the assumption of existence of thermally activated carriers which is given by the expression,[30],

$$\rho = \rho_0 \left(\frac{E_a}{2k_B T} \right), \tag{4}$$

where E_a is the activation energy which is calculated from the linear fit of $\ln \rho$ versus $1/T$ plot. Perceiving a linear variation between $\ln \rho$ and $1/T$ beyond 450 K, all the samples confirm a non-degenerate type of behaviour. The E_a value for pristine sample is estimated as 0.34 eV. For the 50 kGy irradiated sample, there is no change in E_a value. Increase in activation energy for the samples irradiated with 100 kGy and 150 kGy can be associated to their higher resistivity

Table 2 Electrical parameters of Cu_2SnSe_3 irradiated with different electron beam dosages

Irradiation dosage (kGy)	Carrier concentration n (cm^{-3})	Hall mobility μ (cm^2/Vs)	Activation Energy E_a At High temperature regime (eV)	Effective mass m^* (m_e)
0	2.88×10^{20}	13.0	0.34	0.94
50	3.53×10^{20}	9.6	0.34	0.91
100	2.03×10^{20}	12.1	0.37	0.86
150	7.90×10^{19}	5.30	0.38	0.40

**Fig. 3** Secondary electron images of Cu_2SnSe_3 **a** at polished and **b** fractured surfaces. **c** SEM at polished and **d** cross-sectional surface of Cu_2SnSe_3 irradiated with electrons at 150 kGy

as compared to the pristine. The E_a values of pristine and irradiated samples are given in Table. 2. Decrement in the resistivity was observed for the lower dose of electrons (50 kGy), which may be connected to the increase in the Cu vacancies as well as Cu to Sn defects created due to the high-energy electrons. Beyond this, an increase in resistivity is found for the samples irradiated with 100 kGy and 150 kGy, indicating the creation of other types of defects that tend to reduce the acceptor levels. Hall measurements were done at room temperature to have a better

perception into the electrical transport. Positive Hall coefficient of all the samples has clarified the p-type conductivity in all the samples. Carrier density is found to follow the same trend of electrical conductivity, which is comparable with the earlier reported values [31, 32].

Temperature-dependent Seebeck coefficient was measured in the temperature range, 300–700 K which is shown in Fig. 6a. Increase in Seebeck coefficient [$S(T)$] with the increase in temperature signifies the existence of degeneracy in the materials. On the other

hand, resistivity shows a reverse trend with temperature. This may be attributed to the existence of partial degeneracy as reported previously in Cu₂SnSe₃ and isostructural materials [8, 29, 33]. To support the deviation in the thermopower, temperature-dependent Fermi energy and Lorenz number were derived using an algorithm called SPBcal developed by Chang et al. [34] under Java SE runtime environment 1.8.0_131. The equation used for Fermi energy is given by

$$S = \pm \frac{k_B}{e} \left(\frac{2F_1(\eta)}{F_0(\eta)} - \eta \right), \tag{5}$$

where η is the reduced Fermi energy which is linked to Fermi energy E_F as $E_F/k_B T$. $F_0(\eta)$ and $F_1(\eta)$ are Fermi integrals of order $n = 0$ and 1 , respectively. Fermi energy values [see Fig. 7 (b)] are found to be in the range 0.1–0.2 eV, which is considerably smaller than the activation energy as evaluated by thermal activation, thereby validating extrinsic p-type nature of the material. The increased conductivity in 50 kGy is directly related with the increased Fermi energy. Considering the degenerate behaviour of all the samples at near room temperature, density of states effective mass m^* was estimated using Mott’s equation for diffusion thermopower as

$$S(T > \theta_D) = \frac{\pi^2 k_B^2 2m^*}{e\hbar(3n\pi^2)^{2/3}} T, \tag{6}$$

where n is the carrier density, m^* is the effective mass, and e , \hbar , and k_B are electronic charge, Planck’s constant, and Boltzmann constant, respectively. Reduction in m^* values is observed with the increase of irradiation dosage thereby signifying the increased carrier mobility. The Lorenz number (L_0) was further evaluated to support the partial degenerate behaviour in the materials using two different methodologies [34, 35] given by the following equations:

$$L_0 = \frac{k_B^2}{e^2} \frac{(3F_0(\eta)F_2(\eta) - 4F_1^2(\eta))}{F_0^2(\eta)} \tag{7}$$

a

$$L_0 = 1.5 + \exp\left[-\frac{|S|}{116}\right], \tag{8}$$

where the unit of L_0 is $10^{-8} \text{ W}\Omega\text{K}^{-2}$ and S is in μVK^{-1} . Calculated values of L_0 are illustrated in Fig. 7a and b. Both the relations are based on the single parabolic band approximation. The values of L_0 deduced from both the methods are found to be in proximity within the error limits. L_0 values are found to lie above $1.9 \times 10^{-8} \text{ W}\Omega\text{K}^{-2}$ suggesting the partial degenerate behaviour of the samples.

To assess the total charge transport, weighted mobility (μ_w) which is independent of carrier density was computed using Eq. (2). A decrease in μ_w was found with increase in temperature witnessing the heavily doped nature of the materials up to a temperature of about 450 K. Beyond this an increase in μ_w is observed with increase in temperature which may be caused by the rapid enhancement in number of carriers and hence the DOS effective mass m^* . It can be noted that similar temperature behaviour is observed in electrical conductivity in all the samples indicating weighted mobility is one of the major factors controlling the transport behaviour in the present system. The upsurge in the weighted mobility at higher temperatures can be correlated to the partial degeneracy of Cu₂SnSe₃ samples. Power factor ($S^2\sigma$) determined from the electrical properties are found to surge with temperature as shown in Fig. 8b. The results suggest that samples with higher weighted mobility were found to show higher power factor values. Zhang et al. [36] recently proposed a single material parameter ‘ B_E ’ referred to as ‘electronic quality factor’. For a pair of measurements of Seebeck coefficient (S) and electrical conductivity (σ) performed simultaneously at a given temperature, B_E is defined as

$$B_E = S^2\sigma / \left[\frac{S_r^2 \exp(2 - S_r)}{1 + \exp[-5(S_r - 1)]} + \frac{S_r\pi^2/3}{1 + \exp[5(S_r - 1)]} \right], \tag{9}$$

where $S_r = \frac{|S|}{k_B/e}$. This describes the electronic contribution to the power factor. Increased electronic quality factor is accompanied with the increase in power factor. Since the rapid surge in temperature-dependent B_E values is not observed, the possibility of the band convergence is ruled out. Further, the

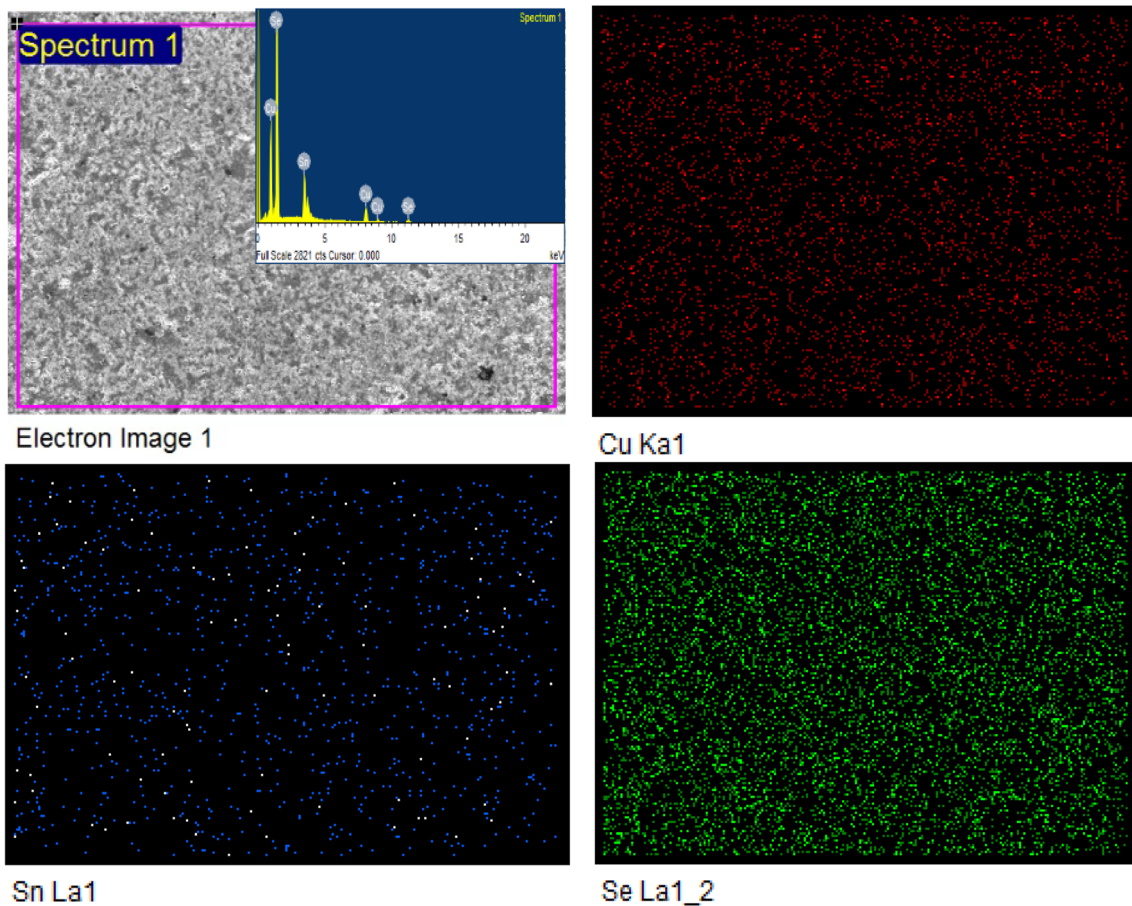


Fig. 4 X-ray elemental mapping with EDX spectra at selected area of Cu_2SnSe_3 sample

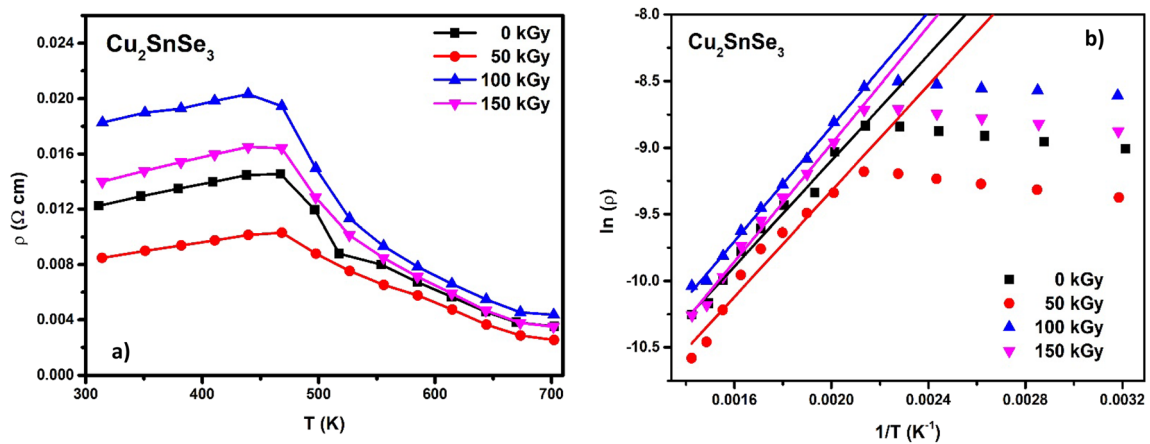


Fig. 5 **a** Temperature-dependent resistivity for pristine and irradiated samples. **b** linear fit to thermal activation model for (Eq. 4) Cu_2SnSe_3 samples irradiated with different dosages

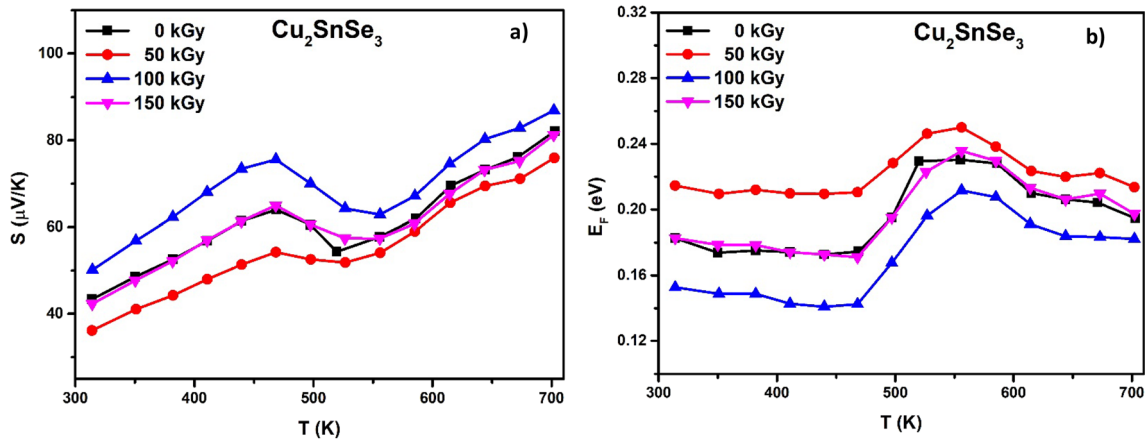


Fig. 6 a Temperature-dependent Seebeck coefficient and b Fermi energy of Cu_2SnSe_3 irradiated with electrons at different dosages

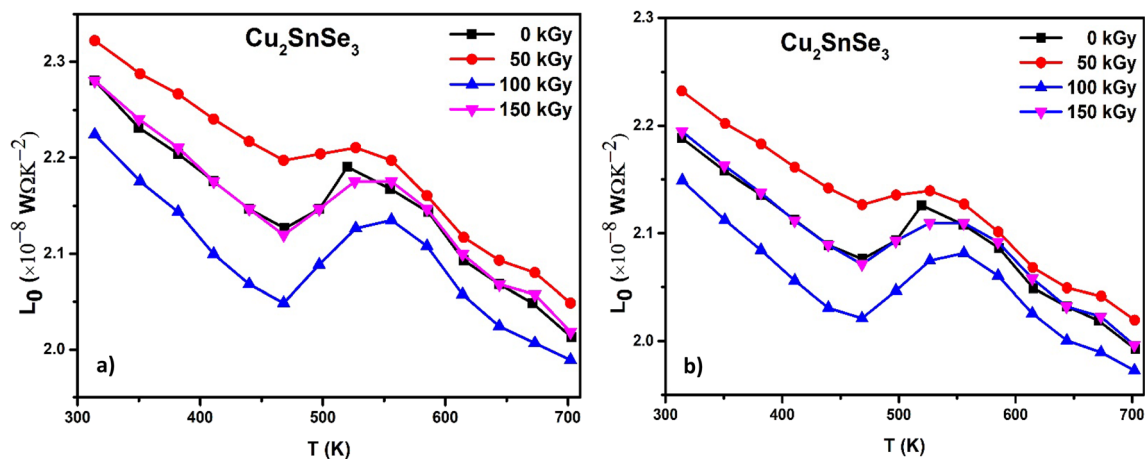


Fig. 7 Temperature-dependent Lorenz number deduced using a Eq. (7) and b Eq. (8) for Cu_2SnSe_3 irradiated with electrons at different dosages

bipolar contribution to the electronic transport is not prompt in the samples at high temperature. Cu_2SnSe_3 irradiated with dosage of 50 kGy is found to achieve the highest power factor of $228 \mu\text{W}/\text{mK}^2$ at 700 K.

4 Conclusion

A systematic study is done on the effect of electron irradiation on the various properties of Cu_2SnSe_3 thermoelectric system synthesised by conventional solid state reaction. All the samples are found to crystallise into cubic sphalerite-type structure and no structural changes are observed in the irradiated

samples. Electrical transport is investigated at near room to mid-temperature regime (300–700 K). A smooth transition from degenerate to non-degenerate type of conductivity is seen in all the samples indicating the injection of minority carriers with ionisation of defects at high temperature. Enhancement of electrical transport is observed at lower electron dosages. Defects created through the knock-on displacement of the constituent atoms enhance the power factor in the material. Cu_2SnSe_3 irradiated with 50 kGy of electrons is found to achieve maximum power factor of $228 \mu\text{W}/\text{mK}^2$ at 700 K which is nearly 20% higher than the power factor of pristine material at 700 K.

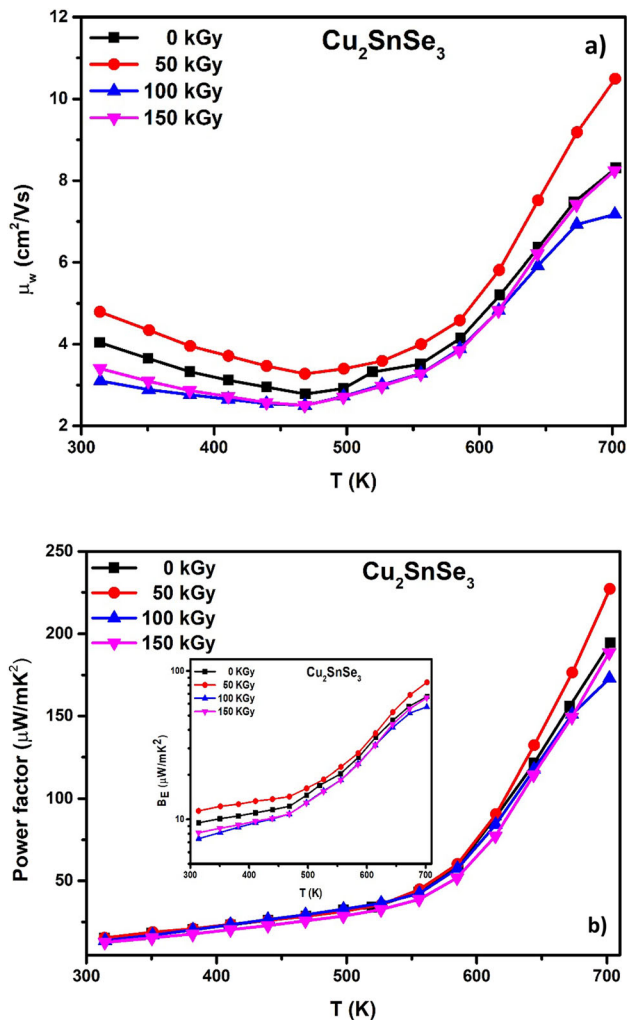


Fig. 8 **a** Temperature-dependent weighted mobility and **b** power factor with inset showing electronic quality factor of Cu_2SnSe_3 irradiated with electrons at different dosages

Acknowledgements

One of the authors (AR) acknowledges DST-FIST Grant (SR/FIST/PS-1/2017/8) and Council of Scientific and Industrial Research Grant [Sanction No.: 03(1409)/17/EMR-II] for the financial support required for this work.

Author contributions

KG: methodology, measurements, and manuscript preparation. SM: methodology. AR: project administration, resources, supervision, and writing review and editing. PP, manuscript preparation. VCP:

resources and methodology. VPV: resources and methodology. JD: resources and methodology.

Funding

Open access funding provided by Manipal Academy of Higher Education, Manipal. This study was funded by DST-FIST Grant (SR/FIST/PS-1/2017/8) and Council of Scientific and Industrial Research Grant [Sanction No.: 03(1409)/17/EMR-II].

Data availability

Data will be made available on reasonable request.

Declarations

Competing interest The authors declare that they have no known competing financial interests or personal relationships that could have appeared to influence the work reported in this paper.

Open Access This article is licensed under a Creative Commons Attribution 4.0 International License, which permits use, sharing, adaptation, distribution and reproduction in any medium or format, as long as you give appropriate credit to the original author(s) and the source, provide a link to the Creative Commons licence, and indicate if changes were made. The images or other third party material in this article are included in the article's Creative Commons licence, unless indicated otherwise in a credit line to the material. If material is not included in the article's Creative Commons licence and your intended use is not permitted by statutory regulation or exceeds the permitted use, you will need to obtain permission directly from the copyright holder. To view a copy of this licence, visit <http://creativecommons.org/licenses/by/4.0/>.

References

1. X. Zhang, L.D. Zhao, Thermoelectric materials: energy conversion between heat and electricity. *J. Mater.* **1**, 92–105 (2015)
2. G.J. Snyder, A.H. Snyder, M. Wood, R. Gurunathan, B.H. Snyder, C. Niu, Weighted mobility. *Adv. Mat.* **2001537**, 1–5 (2020)

3. W. He, B. Qin, L. Zhao.: Predicting the Potential Performance in P-Type SnS Crystals via Utilizing the Weighted Mobility and Quality Factor, *Chin. Phys. Lett.* **8**, 37. 087104 (2020).
4. Y. Li, G. Wang, M. Akbari-Saatlu, M. Procek, H.H. Radamson, Si and SiGe nanowire for micro-thermoelectric generator: a review of the current state of the art. *Front. Mater.* **8**, 1–24 (2021)
5. X. Shi, L. Xi, J. Fan, W. Zhang, L. Chen, Cu-Se.: bond network and thermoelectric compounds with complex diamondlike structure. *Chem. Mater.* **22**, 6029–6031 (2010)
6. H.A. Eivari, Z. Sohbatazadeh, P. Mele, M.H.N. Assadi, Low thermal conductivity: fundamentals and theoretical aspects in thermoelectric applications. *Mater. Today Energy.* **21**, 100744 (2021)
7. M. Siyar, J.Y. Cho, Y. Youn, S. Han, M. Kim, S.H. Bae, C. Park, Effect of annealing temperature on the phase transition, band gap and thermoelectric properties of Cu_2SnSe_3 . *J. Mater. Chem. C* **6**, 1780–1788 (2018)
8. J. Fan, W. Carrillo-Cabrera, L. Akselrud, I. Antonyshyn, L. Chen, Y. Grin, New monoclinic phase at the composition Cu_2SnSe_3 and its thermoelectric properties. *Inorg. Chem.* **52**, 11067–11074 (2013)
9. Y. Li, G. Liu, J. Li, K. Chen, G. He, Z. Yang, Y. Han, M. Zhou, L. Li, Ultrafast one-step combustion synthesis and thermoelectric properties of In-doped Cu_2SnSe_3 . *Mater. Chem. Phys.* **177**, 398–404 (2016)
10. Y. Li, G. Liu, J. Li, K. Chen, L. Li, Y. Han, M. Zhou, M. Xia, X. Jiang, Z. Lin, High thermoelectric performance of In-doped Cu_2SnSe_3 prepared by fast combustion synthesis. *New J. Chem.* **40**, 5394–5400 (2016)
11. Y. Li, G. Liu, T. Cao, L.M. Liu, J. Li, K. Chen, L. Li, Y. Han, M. Zhou, Enhanced thermoelectric properties of Cu_2SnSe_3 by (Ag, In)-Co-doping. *Adv. Funct. Mater.* **26**, 6025–6032 (2016)
12. R. Ma, G. Liu, Y. Li, J. Li, K. Chen, Y. Han, M. Zhou, L. Li, Thermoelectric properties of S and Te-doped Cu_2SnSe_3 prepared by combustion synthesis. *J. Asian Ceram. Soc.* **6**, 1–7 (2018)
13. X. Lu, D.T. Morelli, Thermoelectric properties of Mn-doped Cu_2SnSe_3 . *J. Electron. Mater.* **41**, 1554–1558 (2012)
14. D. Zhao, J. Ning, D. Wu, M. Zuo, Enhanced thermoelectric performance of Cu_2SnSe_3 -based composites incorporated with nano-fullerene. *Materials* **9**, 1–12 (2016)
15. D. Zhao, X. Wang, D. Wu, Enhanced thermoelectric properties of graphene/ Cu_2SnSe_3 composites. *Crystals* **7**, 71 (2017)
16. X. Cheng, Z. Li, Y. You, T. Zhu, Y. Yan, X. Su, X. Tang, Role of cation vacancies in Cu_2SnSe_3 thermoelectrics. *ACS Appl. Mater. Interfaces* **11**, 24212–24220 (2019)
17. K. Gurukrishna, A. Rao, Z.Z. Jiang, Y.K. Kuo, Enhancement of thermoelectric performance by tuning selenium content in the Cu_2SnSe_3 compound. *J. Internet* **122**, 106803 (2020)
18. A.V. Krasheninnikov, K. Nordlund, Ion and electron irradiation-induced effects in nanostructured materials. *J. Appl. Phys.* **107**, 071301 (2010)
19. F. Cheng, A. Li, S. Wang, Y. Lin, P. Nan, S. Wang, N. Cheng, Y. Yue, B. Ge, In situ investigation of the phase transition at the surface of thermoelectric PbTe with van der Waals Control. *Research* **2022**, 1–6 (2022)
20. O. Voigt, B. Krause, P. Pötschke, M.T. Müller, S. Wießner, Thermoelectric performance of polypropylene/carbon nanotube/ionic liquid composites and its dependence on electron beam irradiation. *J. Compos. Sci.* **6**, 25 (2022)
21. H. Gu, G. Li, C. Liu, F. Yuan, F. Han, L. Zhang, S. Wu, Considerable knock-on displacement of metal atoms under a low energy electron beam. *Sci. Rep.* **7**, 1–10 (2017)
22. M. Duchamp, R. Meunier, R. Smajda, M. Mionic, A. Magrez, J.W. Seo, L. Forró, B. Song, D. Tománek, Reinforcing multiwall carbon nanotubes by electron beam irradiation. *J. Appl. Phys.* **108**, 4314 (2010)
23. L. Yao, S. Majumdar, L. Äkäsloppolo, S. Inkinen, Q.H. Qin, S. Van Dijken, Electron-beam-induced perovskite-brownmillerite-perovskite structural phase transitions in epitaxial $\text{La}_{2/3}\text{Sr}_{1/3}\text{MnO}_3$ films. *Adv. Mater.* **26**, 2789–2793 (2014)
24. B. Christopher, A. Rao, B.S. Nagaraja, K. Shyam Prasad, G.S. Okram, G. Sanjeev, V.C. Petwal, V.P. Verma, J. Dwivedi, P. Poornesh, Correlation between structural and transport properties of electron beam irradiated PrMnO_3 compounds. *Solid State Commun.* **270**, 30–37 (2018)
25. M. Takashiri, K. Imai, M. Uyama, H. Hagino, S. Tanaka, K. Miyazaki, Y. Nishi, Comparison of crystal growth and thermoelectric properties of n-type Bi-Se-Te and p-type Bi-Sb-Te nanocrystalline thin films: effects of homogeneous irradiation with an electron beam. *J. Appl. Phys.* **115**, 214–311 (2014)
26. A. Saji, S. Ampili, S.H. Yang, K.J. Ku, M. Elizabeth, Effects of doping, electron irradiation, H^+ and He^+ implantation on the thermoelectric properties of Bi_2Se_3 single crystals. *J. Phys. Condens. Matter* **17**, 2873–2888 (2005)
27. X. Du, M. Takeguchi, M. Tanaka, K. Furuya, Formation of crystalline Si nanodots in SiO_2 films by electron irradiation. *Appl. Phys. Lett.* **82**, 1108–1110 (2003)
28. A. Kumar, P. Dhama, P. Banerji, Enhanced thermoelectric properties in Bi and Te doped p -type Cu_3SbSe_4 compound. *AIP Conf. Proc.* **1942**, 140080 (2018)
29. T. Huang, Y. Yan, K. Peng, X. Tang, L. Guo, R. Wang, X. Lu, X. Zhou, G. Wang, Enhanced thermoelectric performance in

- copper-deficient Cu_2GeSe_3 . *J. Alloys Compd.* **723**, 708–713 (2017)
30. T.T. Lin, S.L. Young, C.Y. Kung, H.Z. Chen, M.C. Kao, M.C. Chang, C.R. Ou, Variable-range hopping and thermal activation conduction of Y-doped ZnO nanocrystalline films. *IEEE Trans. Nanotechnol.* **13**, 425–430 (2014)
31. L. Hu, Y. Luo, Y. Fang, F. Qin, X. Cao, H. Xie, J. Liu, J. Dong, A. Sanson, M. Giarola, X. Tan, Y. Zheng, A. Suwardi, Y. Huang, K. Hippalgaonkar, J. He, W. Zhang, J. Xu, Q. Yan, M.G. Kanatzidis, High thermoelectric performance through crystal symmetry enhancement in triply doped diamondoid compound Cu_2SnSe_3 . *Adv. Energy Mater.* **11**, 210066 (2021)
32. E.J. Skoug, J.D. Cain, D.T. Morelli, Thermoelectric properties of the Cu_2SnSe_3 - Cu_2GeSe_3 solid solution. *J. Alloys Compd.* **506**, 18–21 (2010)
33. W. Li, S. Lin, X. Zhang, Z. Chen, X. Xu, Y. Pei, Thermoelectric properties of Cu_2SnSe_4 with intrinsic vacancy. *Chem. Mater.* **28**, 6227–6232 (2016)
34. K. Chang, C. Liu, An algorithm of calculating transport parameters of thermoelectric materials using single band model with optimized integration. *Comput. Phys. Commun.* **247**, 106875 (2019)
35. H.S. Kim, Z.M. Gibbs, Y. Tang, H. Wang, G.J. Snyder, Characterization of Lorenz number with Seebeck coefficient measurement. *APL Mater.* **3**, 1–6 (2015)
36. X. Zhang, Z. Bu, X. Shi, Z. Chen, S. Lin, B. Shan, M. Wood, A.H. Snyder, L. Chen, G.J. Snyder, Y. Pei, Electronic quality factor for thermoelectrics. *Sci. Adv.* **6**, 6–11 (2020)

Publisher's Note Springer Nature remains neutral with regard to jurisdictional claims in published maps and institutional affiliations.